

Unsupervised Structural Scene Decomposition via Foreground-Aware Slot Attention with Pseudo-Mask Guidance

Huankun Sheng

Tsinghua University

shenghk@tsinghua.edu.cn

Ming Li

Tsinghua University

mingli_thu@tsinghua.edu.cn

Yixiang Wei

Tsinghua University

yx-wei22@mails.tsinghua.edu.cn

Yeying Fan

Tsinghua University

fyydemail@gmail.com

Yu-Hui Wen

Beijing Jiaotong University

yhwen1@bjtu.edu.cn

Tieliang Gong

Xi'an Jiaotong University

adidasgtl@gmail.com

Yong-Jin Liu

Tsinghua University

liuyongjin@tsinghua.edu.cn

Abstract

Recent advances in object-centric representation learning have shown that slot attention-based methods can effectively decompose visual scenes into object slot representations without supervision. However, existing approaches typically process foreground and background regions indiscriminately, often resulting in background interference and suboptimal instance discovery performance on real-world data. To address this limitation, we propose Foreground-Aware Slot Attention (FASA), a two-stage framework that explicitly separates foreground from background to enable precise object discovery. In the first stage, FASA performs a coarse scene decomposition to distinguish foreground from background regions through a dual-slot competition mechanism. These slots are initialized via a clustering-based strategy, yielding well-structured representations of salient regions. In the second stage, we introduce a masked slot attention mechanism where the first slot captures the background while the remaining slots compete to represent individual foreground objects. To further address over-segmentation of foreground objects, we incorporate pseudo-mask guidance derived from a patch affinity graph constructed with self-supervised image features to guide the learning of foreground slots. Extensive experiments on both synthetic and real-world datasets demonstrate that FASA consistently outperforms state-of-the-art methods, validating the effectiveness of explicit foreground modeling and pseudo-mask guidance for robust scene decomposition and object-coherent representation. Code will be made publicly available.

1. Introduction

A fundamental objective in computer vision and representation learning is to interpret visual scenes by identifying and understanding their constituent objects [1, 2]. Object-centric learning (OCL) addresses this goal by decomposing an image into a collection of object-specific latent representations, thereby enabling structured and interpretable scene understanding [3, 4]. Such representations benefit various downstream tasks, including object localization [5] and zero-shot object discovery [1].

Among existing OCL approaches, slot attention (SA) [3, 6–8] has emerged as a prominent framework for unsupervised object-centric representation learning. It iteratively groups visual features into a set of latent slots, each intended to capture a distinct object in the scene. Early SA methods process the entire image in a holistic manner, without explicitly distinguishing foreground from background regions [3]. As a result, in complex real-world images, background textures and illumination variations can distract the attention mechanism, leading slots to capture irrelevant background content rather than foreground objects.

Recent efforts have sought to incorporate implicit cues that encourage slot attention to focus more strongly on foreground regions [6]. While beneficial, these methods only provide implicit, feature-level guidance and lack explicit structural separation between foreground and background, leaving models vulnerable to background interference.

Furthermore, slot representations learned by existing approaches often use a fixed number of slots and suffer from over-segmentation, where a single object is incorrectly split across multiple slots. To mitigate this, GLASS [1] intro-

duces semantic guidance using cross-attention maps from a pre-trained diffusion model [9], which helps align each slot with a complete object region via semantic masks. However, generating these masks requires image captions produced by vision–language models [10], complicating the pipeline and making mask quality highly dependent on the accuracy of generated text descriptions.

To overcome these limitations, we propose **Foreground-Aware Slot Attention (FASA)**, a novel approach that enhances scene decomposition by explicitly focusing on foreground objects while alleviating over-segmentation. FASA first separates the scene into foreground and background components, then decomposes the foreground region into distinct object representations. For foreground–background separation, we introduce two dedicated slots that aggregate features extracted by a Vision Transformer (ViT) [11]. Unlike previous methods that initialize slots randomly, FASA employs a clustering-based initialization strategy, which yields more stable and semantically meaningful slot representations and improves decomposition accuracy. Based on this separation, we design a masked slot attention module where the first slot models the background and the remaining slots capture individual foreground objects. This design enables instance-level segmentation by binding each foreground object to a distinct slot.

Additionally, to optimize the allocation of a fixed number of slots and prevent over-segmentation—especially when the number of foreground instances is smaller than the number of foreground slots—we leverage MaskCut [12] to generate pseudo-masks that guide slot learning. Specifically, these masks are obtained by applying Normalized Cut [13] via a fully connected patch-affinity graph, constructed by computing cosine similarities between self-supervised DINO [14] features extracted from each image patch using a ViT. By incorporating regional information from these masks, slot attention is encouraged to assign patches belonging to the same object to a single slot, thereby preserving object integrity and reducing fragmentation.

In summary, our main contributions are as follows:

- We propose a hierarchical slot attention mechanism that first disentangles foreground and background regions via clustering-based initialization, then refines foreground object decomposition using a masked slot attention strategy. This two-stage design structures representation learning from coarse to fine, enabling robust and precise scene decomposition.
- We introduce robust pseudo masks, derived from a patch-affinity graph of self-supervised visual features, to guide slot representation learning, thereby establishing an effective mechanism to address over-segmentation.
- Experimental results on both synthetic and real-world datasets demonstrate that our method achieves state-of-

the-art performance and exhibits robust generalization on downstream tasks such as object localization and zero-shot object discovery.

2. Related Work

2.1. Unsupervised Object Detection

Recent advances in self-supervised Vision Transformers (ViTs) [11] have demonstrated significant potential for uncovering semantic image structures without human annotation. Notably, DINO revealed that self-supervised ViTs can learn to perform latent semantic segmentation—a capability absent in their supervised counterparts [14]. Inspired by this finding, LOST [15] identified foreground regions without cross-image matching or external supervision, achieving strong performance in single-object detection. TokenCut [13] further extended this paradigm by formulating object detection as a graph partitioning problem. It applied normalized cuts to transformer features within a unified, training-free framework to segment foreground objects in both images and videos, demonstrating performance that substantially outperformed prior approaches.

Beyond single-object detection, FreeSOLO [16] introduced a contrastive self-supervised framework for unsupervised multi-object discovery. Building upon the SOLO architecture [17], it employed a two-stage pipeline: a Free Mask module first extracted coarse object masks, which were then refined through weak supervision and self-training in a subsequent self-supervised SOLO stage. Similarly, MaskDistill [18] directly distilled object masks from transformer attention maps, by clustering them into pseudo-ground truth annotations and refining the results through confidence filtering. CutLER [12] proposed a simple yet effective Cut-and-Learn framework for unsupervised object detection and instance segmentation. It harnessed the inherent object localization capability of self-supervised transformers through MaskCut [12], an algorithm that generated multi-object pseudo-masks, followed by iterative self-training for refinement.

U2Seg [19] unified this evolving field by introducing the first unsupervised universal segmentation framework, capable of performing semantic, instance, and panoptic segmentation within a single model. In parallel, the contrastive saliency network (CSNet) [20] explored unsupervised salient object detection from a representation-learning perspective. Rather than relying on traditional low-level priors such as color or boundary contrast, CSNet introduced a contrastive learning framework that discovers saliency through instance discrimination and feature re-coordination, thereby enabling robust detection of visually distinctive regions without supervision.

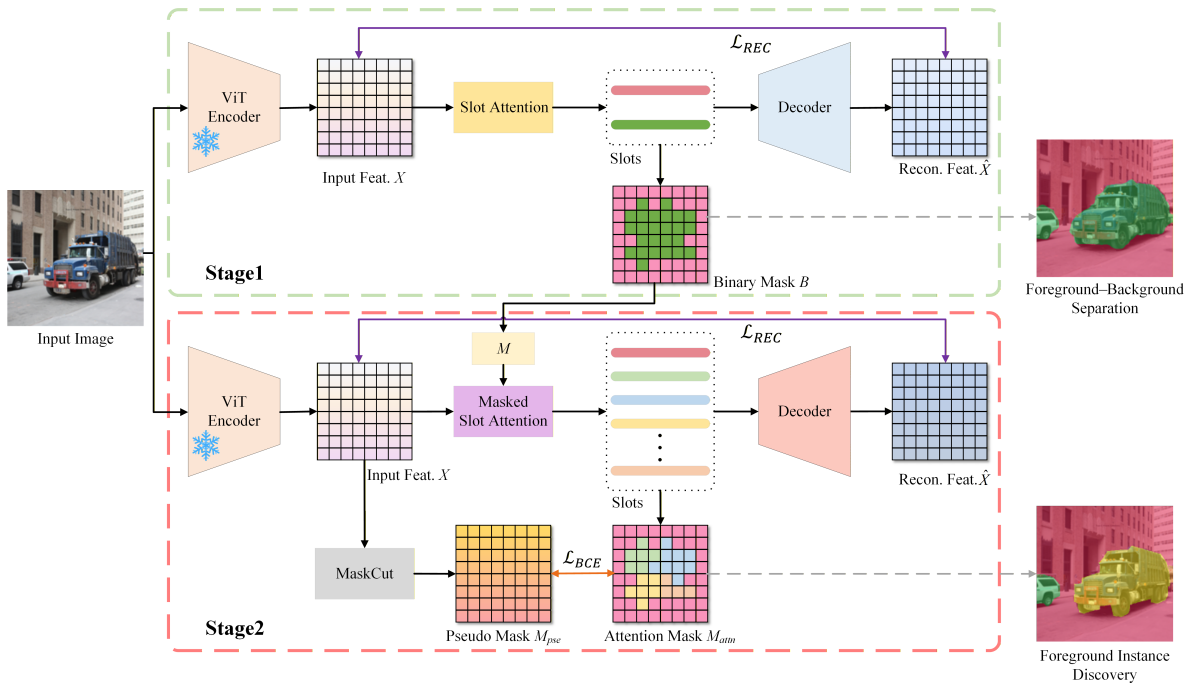


Figure 1. Architecture of the Foreground-Aware Slot Attention (FASA). Our framework operates in two sequential stages. First, a two-slot attention module, trained with feature reconstruction loss, generates a binary mask separating foreground from background regions. Conditioned on this mask, the second stage introduces a masked slot attention mechanism that binds input features to different slots: the first slot is dedicated to representing the background, while the remaining slots correspond to foreground objects. In addition, pseudo labels obtained from MaskCut [12] are used to guide the learning of the foreground slots.

2.2. Object-Centric Learning

Object-centric learning aims to decompose visual scenes into structured, object-level representations. Early approaches such as MONet [21] and IODINE [22] adopted a spatial mixture model paradigm, leveraging sequential attention or iterative variational inference to recover object structure. GENESIS [23] further advanced this line of work by incorporating explicit modeling of latent spatial layouts. However, these methods often depended on recurrent processing or variational optimization, which limited their efficiency and scalability.

In contrast, **slot attention** [3] introduced a simple, differentiable, and end-to-end framework that iteratively binds visual features to a set of latent slots, each intended to capture a distinct object entity. This mechanism has become a foundational component in many subsequent object-centric models [24–28]. Despite its efficiency, traditional slot attention often failed to form coherent object representations in complex real-world scenes. This limitation stemmed primarily from its reliance on pixel-space reconstruction, which provided suboptimal supervisory signals that emphasized low-level visual cues—such as color and texture—at the expense of higher-level semantic content.

To overcome this limitation, recent methods have explored more semantically meaningful training objectives

and architectural improvements. DINOSAUR [8] advanced real-world object-centric learning by reconstructing self-supervised features rather than raw pixels. Similarly, SLATE [29] introduced a transformer-based autoregressive decoder conditioned on object slots, which enabled richer spatial and semantic modeling, while SPOT [7] improved training stability through self-training and patch-order permutation strategies, achieving stronger performance on real-world benchmarks. Parallel efforts such as Adaptive Slot Attention [30] and DIAS [31] refined the slot aggregation mechanism through slot selection or slot re-initialization and self-distillation, leading to improved slot utilization and convergence behavior. GLASS [1] further introduced latent slot diffusion guided by semantic priors to alleviate over- and under-segmentation, though it relied on the accuracy of text descriptions.

The limitation of the aforementioned methods lies in their lack of effective separation of foreground and background, which limited their ability to handle complex real-world scenes, as the reconstruction objectives were easily dominated by low-level visual cues such as color and texture rather than object-level semantics. To address this, FB-Indicator [6] integrated a contrastive foreground-background indicator that injected semantic guidance into slot allocation, reducing background interference

and improving segmentation quality on both synthetic and real datasets. However, this approach still suffered from ambiguous slot assignments and relied on post-processing to correct over-segmentation.

3. Method

This section introduces the proposed FASA model. As illustrated in Figure 1, our approach builds on the slot attention mechanism to enable structured scene decomposition through foreground-background separation and pseudo-mask guidance. We begin by reviewing the fundamentals of slot attention in Section 3.1. Section 3.2 details our hierarchical slot attention design for foreground-background disentanglement. Section 3.3 describes the generation of pseudo-masks for supervision, and Section 3.4 presents the overall loss function used for training.

3.1. Preliminary on Slot Attention

Given an initial set of slots $S^0 \in \mathbb{R}^{K \times D_{\text{slots}}}$ —typically sampled from a Gaussian distribution—slot attention iteratively refines these K latent vectors to aggregate information from the visual tokens $X \in \mathbb{R}^{N \times D_{\text{inputs}}}$, where each slot strives to explain a subset of tokens. For the t -th refinement iteration, the token-to-slot attention is computed as:

$$\text{logits} = \frac{k(X)q(S)^T}{\sqrt{D}}, \quad A = \text{softmax}(\text{logits}) \in \mathbb{R}^{N \times K} \quad (1)$$

where $k(\cdot)$, $q(\cdot)$ are learnable linear transformations that map X and S to a common dimension D , and $\text{softmax}(\cdot)$ is normalized over the slot dimension for each token (row-wise) to encourage competition. Subsequently, the input values are aggregated via a weighted average to derive the updates for each slot:

$$U = W^T v(X) \in \mathbb{R}^{K \times D}, \quad W_{ij} = \frac{A_{ij}}{\sum_i A_{ij}} \quad (2)$$

where $v(\cdot)$ is a linear transformation applied to X . Each slot is then updated by a GRU [32] followed by a multi-layer perceptron (MLP) [33] with a residual connection:

$$S \leftarrow \text{GRU}(S, U), \quad S \leftarrow S + \text{MLP}(\text{LN}(S)) \quad (3)$$

The updated set of slots is then fed into a decoder to reconstruct the input. The decoder can be implemented as a simple MLP [33], a transformer-based model [34], or a diffusion-based decoder [28].

3.2. Foreground-Aware Slot Attention

To obtain semantically coherent object representations, the proposed FASA framework first explicitly separates foreground and background regions. This initial stage aims to disentangle salient foreground areas containing primary objects from less informative background context.

As shown in Figure 1, given the feature map extracted by the encoder, we use two distinct slots to segment the foreground and background within each image. While prior methods [3, 6, 7] typically initialize slots by sampling from a Gaussian distribution $\mathcal{N}(\mu, \text{diag}(\sigma^2))$, we observe that such random initialization often leads to insufficient foreground-background separation after training. Inspired by findings from [13], which demonstrate that ViT features encode semantically rich information suitable for segmentation, we introduce a clustering-based initialization strategy, where the cluster centers derived from ViT features X are used to initialize the slots. Specifically, we apply K-Means++ seeding [35] on X to obtain two centroids $\mu_1, \mu_2 \in \mathbb{R}^D$, which are then mapped to the slot space via a linear transformation to form the two initial slots.

After training, the two slots specialize in representing the foreground and background of the image, respectively. A binary mask is then constructed from the attention map to partition the image into two disjoint sets of patches. To identify which set corresponds to the foreground, we employ a simple yet empirically effective object-centric prior [36], which states that the foreground region contains fewer than two of the four image corners. If this criterion is violated, the assignments of the foreground and background partitions are swapped. The resulting binary mask can be denoted as:

$$B = \{b_i\}_{i=1}^N, \quad b_i \in \{0, 1\} \quad (4)$$

where $b_i = 1$ represents the i -th patch belongs to the foreground, and $b_i = 0$ denotes the background. This separation establishes a structured foundation for subsequent slot-based decomposition over object-relevant regions.

Building on the separation of foreground and background, our FASA framework proceeds to discover and decompose individual objects within the foreground region. In this stage, a new set of learnable slots iteratively attend to distinct objects, enabling unsupervised instance-level decomposition.

For foreground decomposition, a straightforward approach is to apply slot attention directly to the foreground patches. However, since the number of foreground patches varies across images, this results in inconsistent input sizes and unstable training. To address this, we design a masked slot attention module conditioned on the foreground-background separation results. This module explicitly assigns the first slot to represent the background, while the remaining slots model individual foreground objects, thereby enabling structured scene decomposition.

Specifically, we construct a mask $M \in \mathbb{R}^{N \times K}$ based on B . The value of the first column in M is set as:

$$M_{i1} = \begin{cases} +\infty, & \text{if } b_i = 0, \\ -\infty, & \text{if } b_i = 1 \end{cases} \quad (5)$$

where ∞ denotes a large value, e.g., 10^6 , and all other columns of M are set to zero. We then add M to the attention logits in Eq. (1). After applying the softmax operation along the slot dimension, this design enforces the first slot to consistently represent the background, while the remaining slots compete to represent different foreground objects.

3.3. Pseudo Mask Generation

The learned slot representations often suffer from the problems of over-segmentation [1], where patches belonging to the same object are assigned to different slots. To address this issue, we employ pseudo masks to guide the learning of slot representations. Specifically, we generate pseudo masks M_{pse} using the unsupervised MaskCut method [12].

MaskCut discovers multiple objects in an image by iteratively applying Normalized Cuts (NCut) [13] on a patch-affinity graph built from self-supervised ViT features. Given an image, it extracts DINO “key” features for each patch and constructs a fully connected graph with cosine similarities between these features:

$$W_{ij} = \frac{K_i K_j^T}{\|K_i\| \|K_j\|} \quad (6)$$

where K_i is the “key” feature of patch i . NCut then solves the equation $(D - W)x = \lambda Dx$ to obtain a bipartition from the second smallest eigenvector, where D is a $N \times N$ diagonal matrix with $d(i) = \sum_j W_{ij}$. The foreground is then determined from this bipartition using the simple prior [36], as mentioned in Section 3.2. The discovered foreground patches are then masked out, and NCut is reapplied to the masked graph to extract additional object instances. This process typically repeats for three iterations. Full details are provided in the supplementary material.

Once the pseudo ground-truth masks M_{pse} are generated, they are used to guide the slots. Specifically, we extract the attention masks M_{attn} for each slot using the attention matrix from Eq. (1). Each attention mask is then matched to a corresponding component in the pseudo masks M_{pse} , which we formulate as a bipartite matching problem and solve using the Hungarian algorithm [37]. Formally, given O slots with attention masks and pseudo masks M_{pse} containing F segments, we compute a binary assignment matrix $P \in \{0, 1\}^{O \times F}$ as follows:

$$\arg \min_P \sum_{i=1}^O \sum_{j=1}^F -c_{ij} p_{ij} \quad (7)$$

where $p_{ij} \in \{0, 1\}$ indicates whether slot i is matched to segment j . The optimization enforces a one-to-one assignment for each slot. The cost c_{ij} is defined as the mean Intersection-over-Union (IoU) between the predicted mask of slot i and segment j in the pseudo masks M_{pse} .

Guided by the mask generated by MaskCut, slot attention utilizes the regional information from the mask to assign patches belonging to the same object to a single slot, thereby preventing object fragmentation into multiple slots and effectively mitigating the over-segmentation issue.

3.4. Loss Function

In the foreground-background separation stage, we adopt a feature reconstruction loss following [8]. Let $X, \hat{X} \in \mathbb{R}^{N \times D_{\text{inputs}}}$ denote the ground-truth features and their reconstructions. Training minimizes the reconstruction objective:

$$L_{\text{REC}} = \frac{1}{ND_{\text{inputs}}} \|X - \hat{X}\|_2^2 \quad (8)$$

In the foreground decomposition stage, we optimize a combined objective consisting of the feature reconstruction loss L_{REC} and a binary cross-entropy loss L_{BCE} between the pseudo mask M_{pse} and the attention mask from the slots M_{attn} . The binary cross-entropy loss is only computed on the matched slots, according to the matching matrix $P \equiv P(M_{\text{pse}}, M_{\text{attn}})$. The full loss is given by:

$$L = L_{\text{REC}} + \lambda L_{\text{BCE}}(P(M_{\text{pse}}, M_{\text{attn}})) \quad (9)$$

4. Experiment

4.1. Setup

Datasets. We evaluate our method on both synthetic and real-world datasets. For synthetic evaluation, we adopt the MOVIC [38], which contains approximately 1,000 realistic 3D-scanned objects distributed across scenes with 3–10 objects each. Following the practice in [8], we randomly sample frames from this video-based dataset for our experiments. For real-world evaluation, we use MS COCO 2017 [39], which contains diverse natural images with multiple co-occurring objects, making it a challenging benchmark for object-centric methods. We also include PASCAL VOC 2012 [40], which typically features one or a few dominant objects per image and therefore provides a more straightforward evaluation setting. In addition, we evaluate the zero-shot generalization capability of our model using the CLEVRTex [41] and Obj365 [42] datasets.

Metrics. We evaluate object-centric learning performance using Mean Best Overlap (mBO) and Mean Intersection-over-Union (mIoU). The mBO metric is computed at two levels—instance-level (mBOⁱ) and category-level (mBO^c)—by pairing each predicted mask with the ground-truth instance or semantic mask that yields the highest overlap. For mIoU, the predicted masks are first aligned with the ground-truth annotations using the Hungarian assignment algorithm to ensure optimal one-to-one matching before computing the intersection-over-union scores.

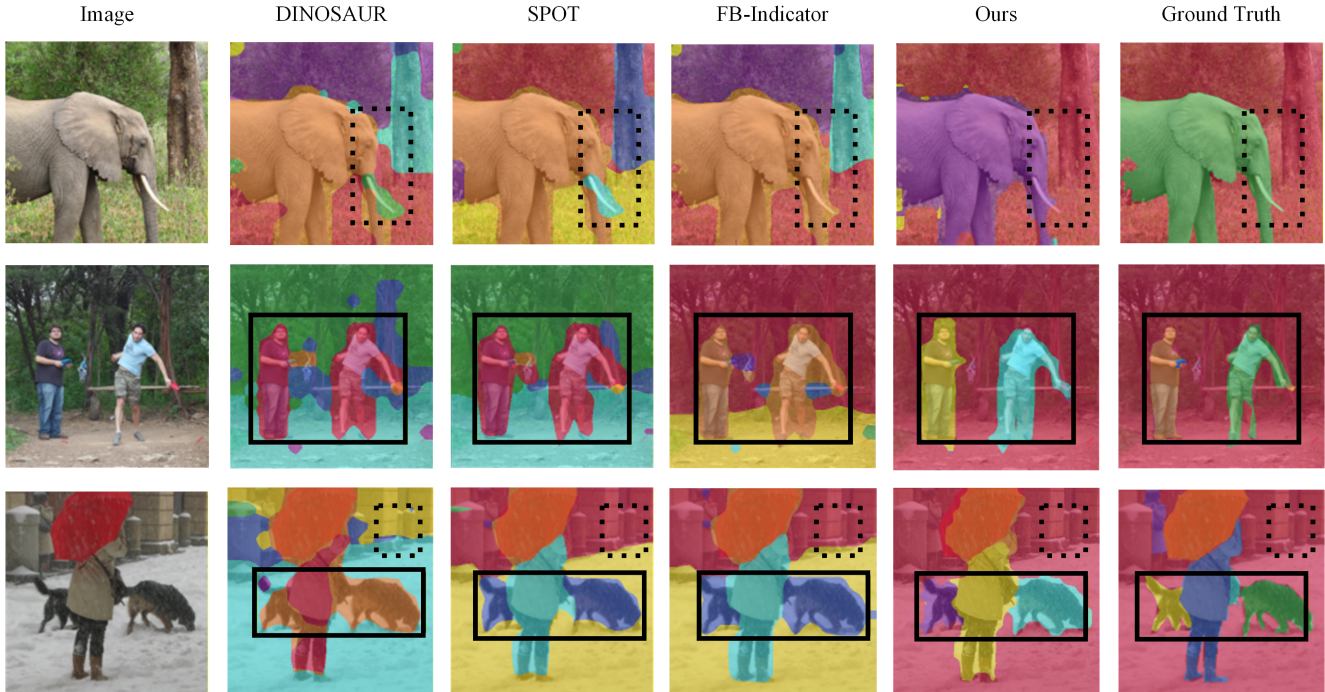


Figure 2. Qualitative comparisons of object discovery. Existing methods tend to over-segment both background regions and foreground objects, as indicated by the dashed boxes. They also struggle to achieve precise instance-level decomposition, as highlighted by the solid boxes. In comparison, our method produces object masks that align closely with the ground-truth annotations.

Implementation Details. We train our model using the Adam optimizer with parameters $\beta_1 = 0.9$, $\beta_2 = 0.999$, no weight decay, and a batch size of 64. The initial learning rate is set to 0.001, following a linear warm-up for the first 10,000 optimization steps and a cosine decay schedule thereafter. The model is trained in two stages, with COCO and PASCAL trained for 100 and 300 epochs, and MOVi-C for 50 and 100 epochs, respectively. We adopt a ViT-S/14 encoder initialized with DINOv2 [43] and an MLP decoder. Unless otherwise specified, the binary cross-entropy (BCE) loss is weighted by $\lambda = 0.05$. Following [7], the number of slots is set to 7, 6, 11 for COCO, PASCAL, MOVi-C, respectively. All experiments are conducted on a single RTX 3090Ti GPU. Additional implementation details are provided in the supplementary material.

4.2. Comparison with Object-Centric Methods

Table 1 summarizes the quantitative performance of different methods on the COCO, PASCAL, and MOVi-C benchmarks. Our method consistently outperforms representative baselines [3, 6–8, 27, 29, 31] in terms of the mIoU and instance-level mBO metrics across all datasets, demonstrating that explicit foreground decomposition combined with pseudo-mask guidance enhances both object discovery and segmentation accuracy.

Figure 2 provides qualitative comparisons of object dis-

Table 1. Comparison of different methods on MOVi-C, COCO, and VOC datasets.

Model	MOVi-C		COCO			VOC		
	mIoU	mBO ⁱ	mIoU	mBO ⁱ	mBO ^c	mIoU	mBO ⁱ	mBO ^c
SA [3]	–	26.3	–	17.2	19.2	–	24.6	24.9
SLATE [29]	37.8	39.4	–	29.1	33.6	–	35.9	41.5
DINOSAUR [8]	41.8	42.4	31.6	33.3	41.2	42.0	43.2	47.8
StableLSD [27]	44.2	45.6	24.7	25.9	30.0	31.5	32.1	35.4
SPOT [7]	46.4	47.0	33.0	35.0	44.7	48.8	48.3	55.6
DIAS [31]	–	–	30.1	32.8	–	42.8	44.8	–
FB-Indicator [6]	47.8	49.0	–	35.7	45.3	–	49.3	56.5
Ours	48.2	49.5	34.1	36.5	43.9	49.5	50.2	57.3

covery results. Our method shows superior capability in both scene decomposition and foreground object discovery, effectively separating foreground objects from background regions to produce accurate and structurally coherent scene representations. Furthermore, it exhibits enhanced robustness in identifying salient objects while suppressing interference from cluttered backgrounds in an instance-centric manner, enabling precise object localization even in visually complex environments.

In contrast, competing methods reveal notable limitations when processing challenging scenes. They frequently fragment background regions into multiple disjoint segments and suffer from under-segmentation, where distinct objects are incorrectly merged into single regions. Additional results are provided in the supplementary material.

4.3. Discussion and Ablation Study

Separation of Foreground and Background. We evaluate the effectiveness of different methods in performing foreground–background separation. Table 2 reports quantitative results, with visual comparisons provided in Figure 3. For DINOSAUR, SPOT, FB-Indicator, and our method, we fix the number of slots to two. For k-means++, we similarly use two clustering centroids. Following [6], we adopt Mean Best Overlap (mBO) as the evaluation metric. In our experiment, ground-truth masks are binarized into foreground (1) and background (0), and predictions are matched to ground truth via best-overlap matching strategy.

Table 2. Comparison of different methods on foreground and background separation.

Model	VOC	COCO
DINOSAUR (2 slots) [8]	47.6	46.9
SPOT (2 slots) [7]	50.8	46.4
FB-Indicator (2 slots) [6]	52.6	48.4
k-means++ [35]	47.5	43.6
Ours	60.1	51.8

As shown in Table 2, our method achieves the best performance on both COCO and PASCAL datasets, demonstrating the advantage of our clustering-based initialization strategy in producing accurate and stable foreground–background separation. In contrast, while baselines such as DINOSAUR and SPOT can partition scenes into two regions, they often fail to precisely separate foreground from background. Visual results in Figure 3 further illustrate that these methods frequently include background areas in foreground predictions, whereas our approach cleanly distinguishes object regions. Although FB-Indicator and standalone k-means++ also separate foreground and background to some extent, our method consistently outperforms them in both qualitative and quantitative evaluations. More visualization results are included in the supplementary material.

Unsupervised salient object detection. We further compare our method with state-of-the-art unsupervised salient object detection techniques [5, 12, 13, 44–46]. Table 3 summarizes results on the PASCAL-S dataset [47], evaluated using pixel accuracy (Acc), intersection-over-union (IoU), and F_β score as in [5]. Our method achieves competitive or superior performance across all metrics, indicating its effectiveness in capturing foreground saliency and establishing a reliable basis for subsequent object-level decomposition.

Impact of Pseudo-Mask Guidance. We conduct an ablation study to evaluate the contribution of pseudo-mask guidance by removing the corresponding loss term during

Table 3. Comparison of different methods on object localization.

Model	Acc	IoU	F_β
TokenCut [13]	89.7	67.5	0.782
UMNET [44]	89.6	63.9	0.771
SelfMask [45]	90.1	69.6	0.806
CutLER [12]	89.1	67.7	0.764
Found [5]	91.3	71.5	0.815
3SD [46]	90.6	69.1	0.791
Ours	91.7	72.3	0.809

Table 4. The effect of pseudo-mask guidance.

Loss term	mIoU	mBO ⁱ	mBO ^c
<i>w/o</i> \mathcal{L}_{BCE}	25.2	26.8	30.5
<i>w/</i> \mathcal{L}_{BCE}	34.1	36.5	43.9

training on the COCO dataset. As shown in Table 4, the variant *w/o* \mathcal{L}_{BCE} exhibits significant performance degradation. More critically, qualitative results in Figure 4 reveal that without pseudo-mask guidance, the model becomes prone to over-segmenting foreground objects. This occurs because the slots compete to parse the foreground objects independently. When the number of objects in the foreground is small, this competition causes the slots to partition a single object into multiple fragments, thereby resulting in over-segmentation. Additional analysis is provided in the supplemental material.

Effect of Different Slot Numbers. The number of slots influences the model’s capacity to discover and represent multiple objects in complex scenes. To evaluate this effect, we conduct experiments using varying slot configurations. As summarized in Table 5, optimal performance on COCO and VOC datasets is achieved with 7 and 6 slots respectively, indicating that dataset characteristics influence the ideal slot configuration.

Table 5. Effects of different K values.

Dataset	K	mIoU	mBO ⁱ	mBO ^c
COCO	5	30.3	31.6	35.4
	6	32.6	34.5	41.9
	7	34.1	36.5	43.9
	8	33.7	36.9	43.7
	9	32.8	34.9	40.3
VOC	5	46.6	50.3	53.5
	6	49.5	50.2	57.3
	7	48.9	49.3	52.5
	8	46.9	47.3	51.8
	9	45.2	46.9	49.1

4.4. Downstream Applications

To further evaluate the effectiveness and generalization capability of the learned slot representations, we investigate

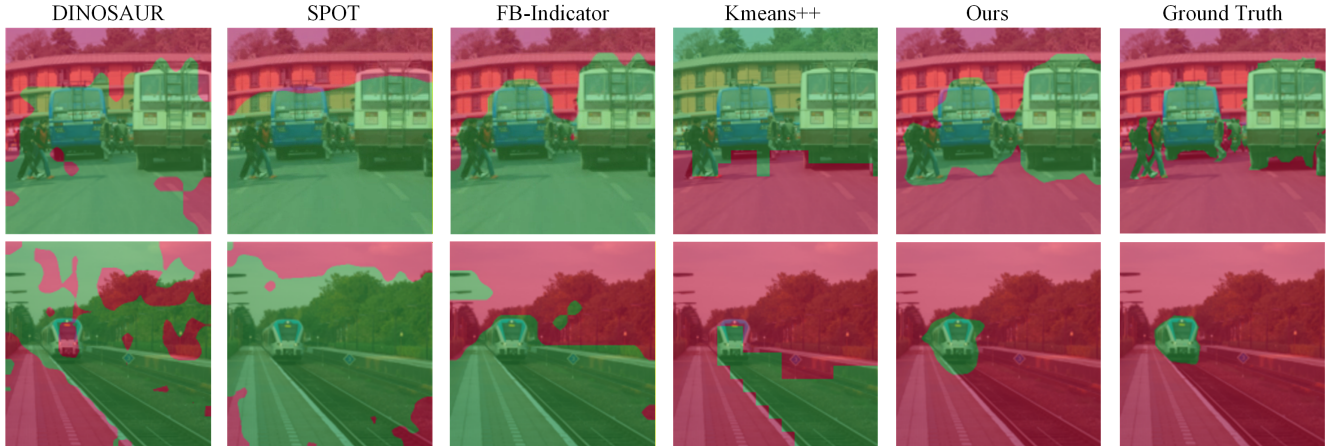


Figure 3. Visual comparison of foreground–background separation. Green regions denote detected foreground; red regions indicate background. Our method achieves more accurate structural separation between foreground objects and background areas, generating masks that align closely with ground-truth annotations.



Figure 4. Visualization of results with and without pseudo-mask supervision. (a) Without pseudo-mask supervision; (b) With pseudo-mask supervision. Using pseudo-mask supervision can effectively reduce over-segmentation.

two downstream tasks: object localization [5] and zero-shot object discovery [1].

Table 6. Comparison on the object localization task.

Model	VOC	COCO
DINOSAUR [8]	0.047	0.071
StableLSD [27]	0.045	0.067
SPOT [7]	0.042	0.064
FB-Indicator [6]	0.044	0.066
Ours	0.038	0.061

Object Localization. This task involves predicting an object’s bounding box center from its corresponding slot representation. Following [8], we evaluate on COCO and PASCAL VOC datasets using mean squared error (MSE) as the evaluation metric. As shown in Table 6, our method achieves superior localization accuracy. The results con-

firm that our learned slot representations encode spatially coherent object information, enabling more precise position estimation through effective instance-level representations.

Table 7. Comparison on the zero-shot object discovery task.

Model	CLEVRTex		Obj365	
	mIoU	mBO ⁱ	mIoU	mBO ⁱ
DINOSAUR [8]	30.2	35.1	16.2	18.9
StableLSD [27]	24.0	27.6	14.8	16.9
SPOT [7]	39.5	43.7	18.0	20.7
FB-Indicator [6]	39.7	44.2	18.2	20.8
Ours	40.6	44.9	18.4	21.3

Zero-Shot Object Discovery. This task evaluates a model’s ability to discover objects in unseen datasets. We train our model on COCO and evaluate its generalization performance on CLEVRTex [41] and Objects365 [42] datasets. As shown in Table 7, our approach outperforms existing methods. By learning foreground-biased slot representations, our method produces more accurate instance-level segmentation masks, demonstrating strong generalization capability for zero-shot object discovery.

5. Conclusion

In this work, we introduced Foreground-Aware Slot Attention (FASA), a two-stage framework designed to enhance unsupervised scene decomposition through explicit foreground–background separation. By integrating dual-slot competition with clustering-based initialization, FASA achieves structured scene representations while mitigating background interference. The proposed masked slot attention mechanism enables fine-grained foreground ob-

ject discovery, guided by a pseudo-mask to prevent over-segmentation. Extensive experiments on both synthetic and real-world datasets confirm that FASA consistently outperforms existing methods.

Limitations and Future Work. Despite its strong performance, our approach shares certain limitations with existing object-centric methods. It struggles in crowded scenes containing numerous similarly appearing objects, where instance-level discrimination remains challenging. Additionally, the model shows limited sensitivity to small, spatially isolated objects, which may be overlooked or absorbed into background representations. We provide an analysis of these failure cases in the supplementary material. Future work will focus on enhancing discrimination in dense scenes and improving small-object awareness.

Unsupervised Structural Scene Decomposition via Foreground-Aware Slot Attention with Pseudo-Mask Guidance

Supplementary Material

A. Implementation Details

A.1. Slot Initialization

In the first-stage *foreground-background separation*, the encoder features are clustered into two groups, and the resulting cluster centers are used to initialize the two slots. To obtain a stable and well-separated initialization, we employ the K-Means++ strategy [35], which randomly selects the first center and then iteratively samples subsequent centers with probabilities proportional to their squared distances from the existing centers. Subsequently, we apply the standard K-Means algorithm, in which each feature is assigned to its nearest cluster center, and the centers are iteratively updated as the mean of their assigned samples until convergence. The resulting cluster centers are then projected to the predefined slot dimension D_{slots} via a linear transformation layer to ensure compatibility with the slot representations. In our implementation, we set $D_{\text{slots}} = 256$.

For the second-stage *foreground decomposition*, the initial set of K slots are randomly sampled from a Gaussian distribution parameterized by learnable mean $\mu \in \mathbb{R}^{D_{\text{slots}}}$ and log standard deviation $\log \sigma \in \mathbb{R}^{D_{\text{slots}}}$.

A.2. Implementation of Slot Attention

Our slot attention implementation is based on the formulation of Locatello et al. [3]. We begin by normalizing the N input features and projecting them into the slot space via a two-layer MLP, resulting in features of dimension D_{slots} . The model initializes slot vectors by clustering (first stage) or sampling from a Gaussian distribution (second stage). During iterative updates, each step includes: (1) normalizing the slot representations, (2) performing attention to assign input features to slots, (3) updating slot states through a GRU [32], and (4) applying a residual two-layer MLP. The query, key, and value projections all have dimensionality $D_{\text{slots}} = 256$ and omit bias terms. The MLP used in this process has a hidden dimension of $4 \times D_{\text{slots}}$.

A.3. MLP Decoder

Our MLP-based decoder adopts the spatial broadcast mechanism from prior studies [33][8]. Each slot is expanded into N tokens that represent image patches, and augmented with learnable positional embeddings for spatial reference. These tokens are independently processed by a four-layer MLP with ReLU activations, producing both a reconstruction vector and an alpha (attention) map per slot. The alpha map identifies the spatial regions activated by each slot.

The final feature reconstruction is generated by combining all slot reconstructions, where alpha maps act as weighting coefficients.

A.4. MaskCut

In practice, we construct the binary similarity matrix W in Eq. 6 by applying a threshold of $\tau = 0.15$. Elements satisfying $W_{ij} < \tau$ are replaced with 1×10^{-5} , while those satisfying $W_{ij} \geq \tau$ are assigned a value of 1.

MaskCut generate multiple object masks in an image by iteratively applying Normalized Cuts (NCut) [13] on the similarity matrix W . Once the bipartition is obtained via NCut at iteration t , we derive two disjoint patch groups and construct a foreground mask M^t . Specifically, $M_i^t = 1$ if $x_i > \text{mean}(x^t)$, indicating foreground, and $M_i^t = 0$ otherwise, indicating background. The vector x^t is the eigenvector associated with the second smallest eigenvalue λ as illustrated in Section 3.3.

We reverse the partitioning of the foreground and background, i.e., $M_i^t = 1 - M_i^t$, if the foreground set should contain more than two of the four corners. We then mask out the discovered foreground using the foreground mask:

$$W_{ij}^{t+1} = \frac{\left(K_i \prod_{s=1}^t \hat{M}_i^s\right) \left(K_j \prod_{s=1}^t \hat{M}_j^s\right)}{\|K_i\|_2^2 \|K_j\|_2^2} \quad (\text{S1})$$

where $\hat{M}_i^s = 1 - M_i^s$, K_i is the "key" feature of patch i .

By iteratively performing NCut [13] and removing the discovered foreground regions from the similarity matrix W at each iteration, multiple object masks can be extracted from a single image. Following CutLER [12], we set the number of iterations to $n = 3$.

A.5. Training Details

Our FASA (Foreground-Aware Slot Attention) framework employs a ViT-S/14 encoder initialized with DINOv2 [43], omitting the final layer normalization. In the MLP-based decoder, the hidden layer size is set to 2048. Across all experiments, the slot attention module is iterated three times, with a slot dimension of 256 and an MLP hidden dimension of 1024. We use the Adam optimizer with parameters $\beta_1 = 0.9$ and $\beta_2 = 0.999$, no weight decay, and a batch size of 64.

Our training pipeline is divided into two stages. In stage 1, we optimize the foreground-background separation module illustrated in the upper portion of Fig. 1. Once trained, this module is frozen. In stage 2, we train the foreground

decomposition module shown in the lower portion of Fig. 1. For both stages, the learning rate follows a linear warm-up from 0 to its peak value over 10,000 iterations, followed by cosine annealing decay. For experiments on COCO [39] and PASCAL VOC [40], the peak learning rate is set to 1×10^{-4} and the minimum value to 1×10^{-7} . For MOVi-C [38] experiments, the peak learning rate is 2×10^{-4} and the minimum value is 1×10^{-5} .

B. More Experimental Results

B.1. Comparison between Transformer Decoder and MLP Decoder

Table S1. Comparison between different decoders.

Decoder	mIoU	mBo ⁱ	mBo ^c
Transformer	32.3	34.1	39.7
MLP	34.1	36.5	43.9

In this study, we adopt an MLP decoder, as it is more effective at facilitating instance-level scene decomposition [8][1]. To further examine the influence of decoder design, we compare the MLP decoder with a Transformer-based decoder on the COCO dataset. The quantitative results are summarized in Table S1. We observe that the MLP decoder outperforms its Transformer-based counterpart, highlighting its advantage within our framework.

B.2. Comparison with Different Pre-trained Image Features

Table S2. Evaluation with various pre-trained encoders on COCO.

Encoder	mIoU	mBo ⁱ	mBo ^c
DINOv1 [14]	32.5	34.2	42.8
MOCO-v3 [48]	30.6	31.5	40.1
MAE [49]	31.9	33.7	41.2
Ours	34.1	36.5	43.9

In our study, we adopt DINOv2 [43] as the image encoder. To further understand how different pre-training strategies affect the performance of our framework, we additionally conduct experiments on the COCO dataset using features extracted from several alternative self-supervised models, including DINOv1 [14], MOCO-v3 [48], and MAE [49]. As reported in Table S2, our method consistently achieves the best results when DINOv2 is used, outperforming the other pre-trained encoders by a clear margin. Based on this observation, we choose DINOv2 as the backbone for all subsequent experiments, given its superior representational quality and strong compatibility with our object discovery framework.

B.3. Comparison with FG-ARI Scores

Table S3. Comparison between OCL methods for the FG-ARI metric.

Model	VOC	COCO
SA [3]	12.3	21.4
SLATE [29]	15.6	32.5
DINOSAUR [8]	24.8	34.3
StableLSD [27]	8.7	35.0
SPOT [7]	19.9	37.8
FB-Indicator [6]	25.0	38.1
Ours	25.6	38.7

FG-ARI, a foreground-focused variant of the adjusted Rand index (ARI) [50], measures clustering similarity in a permutation-invariant manner while evaluating only the foreground regions of an image. FG-ARI has been a common metric in assessing predicted object masks against ground-truth segmentation in previous works [7][23][41]. However, FG-ARI can be unreliable because it disregards background pixels and does not adequately reflect the structural accuracy of predicted masks [7][1]. We also report FG-ARI results in Table S3 for completeness and comparability with previous studies. The results show that our method attains the highest performance, which we attribute to its ability to accurately capture and isolate foreground objects.

B.4. Analysis of Loss Weight λ

To evaluate the impact of the parameter λ in Eq. 9, we conduct an ablation study by varying λ across several settings on the COCO dataset. The experimental results are presented in Table S4. The model achieves its optimal performance at $\lambda = 0.05$. As λ decreases, the reconstruction loss L_{REC} begins to dominate the training objective, leading to over-segmentation of foreground objects. In contrast, an excessively large λ overweights the L_{BCE} term, causing the number of foreground slots to collapse to the number of objects indicated by the pseudo mask (i.e., $n = 3$). This restricts the model’s ability to discover additional objects and ultimately results in under-segmentation.

B.5. Object Localization

For the object localization task, we employ a single-layer linear model for predicting object positions. We follow the approach in [8] to associate labels with their corresponding slots. Optimization is performed using AdamW [51] with a fixed learning rate of 3×10^{-4} . Image coordinates are normalized to the range $[0, 1]$ by dividing by the image dimensions.

Table S4. Effect of the loss weight λ on COCO.

λ	mIoU	mBo ⁱ	mBo ^c
1	26.3	28.3	37.9
0.5	29.2	31.1	38.7
0.05	34.1	36.5	43.9
0.005	30.5	32.6	39.2
0	25.2	26.8	30.5



Figure S1. Visualization of zero-shot object discovery. Our approach exhibits strong generalization capabilities across both synthetic datasets and challenging real-world image datasets, maintaining robust performance even on data that significantly deviates from the training distribution.

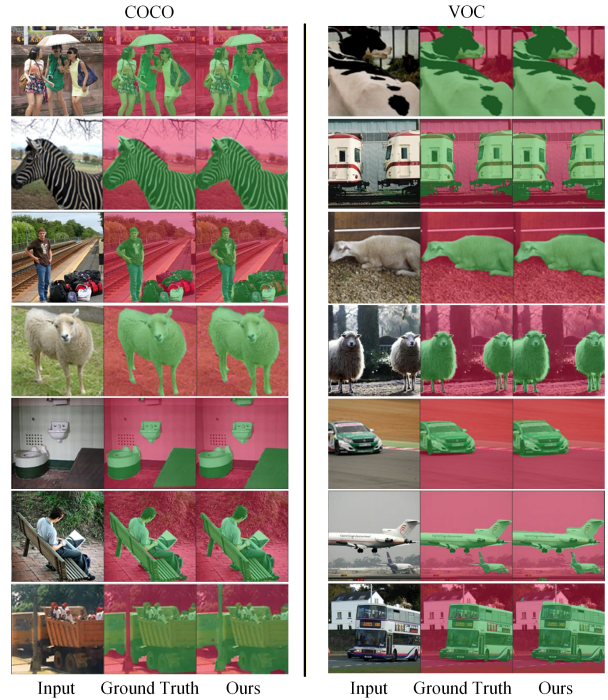


Figure S2. Visualization of foreground-background separation. In the figure, red denotes the background, and green denotes the foreground. Our method accurately detects the objects in the foreground and produces results that are close to the ground truth.

B.6. More Details on Zero-Shot Object Discovery Task

For the zero-shot object discovery task, we train our model on COCO and evaluate its generalization ability on the test sets of the CLEVRText [41] and Objects365 [42] datasets. CLEVRText is a texture-rich synthetic dataset designed for unsupervised multi-object segmentation. It incorporates realistic textures, materials, and lighting variations, yielding scenes that better approximate real-world visual complexity. In CLEVRText, each image contains 3–10 objects, and we use 10 slots for object discovery. Objects365 is a large-scale dataset for generic object detection, consisting of approximately 600K images and 10 million annotated bounding boxes across 365 categories. It provides highly diverse real-world scenes, making it a strong benchmark for assessing cross-dataset generalization. Since ground-truth masks are not available, we obtain the masks for Objects365 using SAMv2 [52], and we use 7 slots for evaluation on this dataset.

Fig. S1 presents zero-shot object discovery results of our method on the two datasets described above. These visualization results show that our approach exhibits strong generalization ability across datasets and scenes.

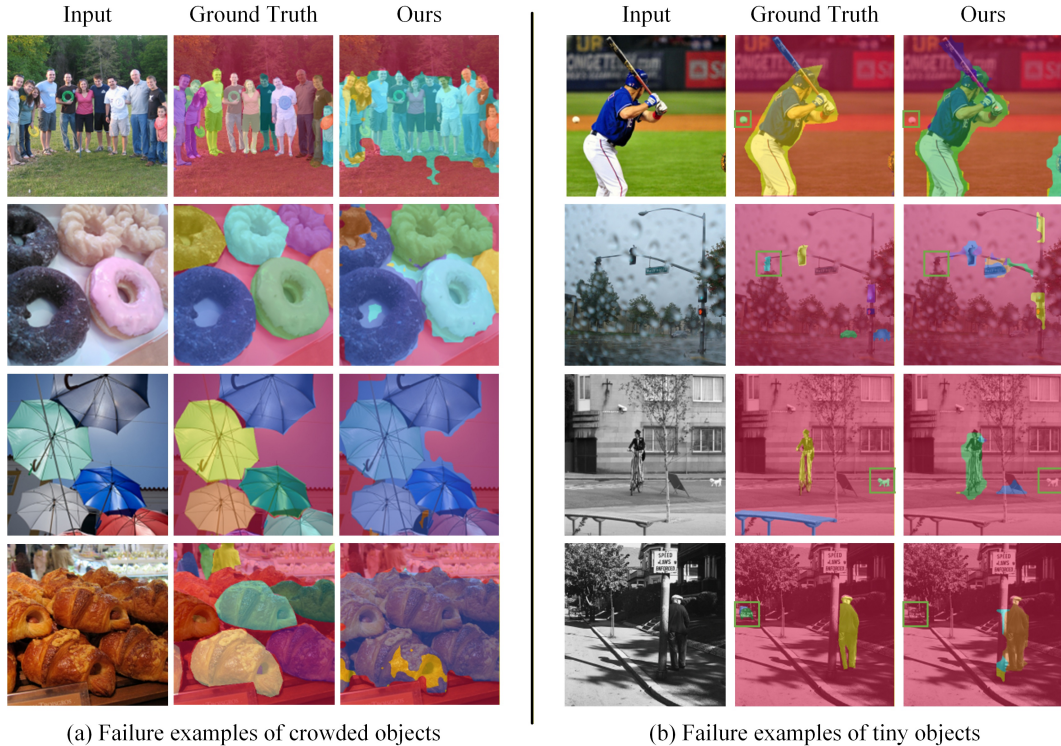
On the CLEVRText dataset, our method adaptively han-



Figure S3. Visualization of object discovery. The red regions represent the background, whereas the other colors denote different foreground objects, each assigned to a separate slot. Our method is capable of producing instance-level object discovery results, yielding outputs that closely match the ground-truth annotations.

dles diverse background variations and complex object compositions. Despite differences in background textures, lighting conditions, and object counts or spatial arrangements, our model consistently produces object regions that closely align with the ground truth. It accurately identifies and localizes the primary instances in each image, demonstrating robustness to previously unseen visual patterns.

On the Objects365 dataset, our method achieves strong performance in more challenging real-world settings. Even in natural images containing substantial noise, complex occlusions, and large variations in object scale, our model can still precisely differentiate individual instances and achieve reliable instance-level binding. This highlights the method's adaptability and stability when applied to real-



(a) Failure examples of crowded objects

(b) Failure examples of tiny objects

Figure S4. Failure examples. Our method struggles to achieve instance-level segmentation in highly crowded scenes. In addition, small objects may sometimes be merged into the background, as indicated by the green boxes.

world scenes.

Overall, these results demonstrate that our method generalizes effectively to out-of-distribution data and maintains stable performance under diverse and challenging conditions, reflecting strong generalization capability, robustness, and practical applicability.

B.7. More Visualization Results

We provide additional visualization results to further validate the effectiveness of our method.

Fig. S2 presents the foreground object detection results of our approach on the COCO and VOC datasets. As illustrated in the figure, our method demonstrates strong robustness across diverse visual scenes. Even in images containing cluttered backgrounds, varying illumination conditions, or multiple interacting instances, the model is able to reliably distinguish foreground objects from their surrounding context. It not only identifies the primary objects with high accuracy but also preserves fine-grained structural details, producing sharp and precise object boundaries. These results further validate the effectiveness of our approach in handling real-world scenarios and underscore its capability for accurate foreground extraction in challenging environments.

Fig. S3 shows the object discovery results of our method

on the COCO and VOC datasets. From the figure, we can observe that our approach demonstrates strong robustness in complex visual environments. On the one hand, it effectively separates the foreground from the background, preventing cluttered or textured backgrounds from interfering with the slot assignment process. This allows foreground slots to concentrate more precisely on the salient foreground regions, thereby improving the overall quality of object discovery. On the other hand, our method successfully achieves instance-level binding of foreground objects. It is able to assign different objects belonging to the same semantic category to distinct slots, while simultaneously avoiding unnecessary over-segmentation of individual instances. These results highlight the capability of our approach to capture fine-grained object structures and maintain coherent instance representations even in challenging real-world scenes.

B.8. Analysis of Failure Cases

Fig. S4 presents several failure cases of our method. As shown in Fig. S4 (a), our approach struggles to achieve instance-level object discovery in highly crowded scenes—an issue commonly observed in slot attention-based models. This limitation can be attributed to several factors. First, slots are global latent representations that

do not explicitly encode object boundaries, geometric structures, or occlusion relationships. Consequently, when objects are densely packed or heavily occluded, the attention mechanism has difficulty assigning spatially continuous regions to distinct slots. Second, our method is trained in a fully unsupervised setting without semantic or structural priors, making it challenging to distinguish adjacent objects with similar appearance or shape. Finally, the information from multiple objects can become highly entangled on the feature map. This exacerbates the difficulty of separating individual instances and often results in under-segmentation or incorrect merging in crowded scenes.

As shown in Fig. S4 (b), our method may fail to detect extremely small objects. This limitation primarily arises from the low visual saliency of such tiny instances: their appearance often contains only a few pixels with weak contrast against the background. As a result, these objects are easily absorbed into surrounding background regions during the foreground-background separation stage, causing the model to overlook them or fail to assign them to dedicated slots. This observation suggests that enhancing sensitivity to fine-scale details could further improve the method's performance on scenes containing tiny objects.

References

- [1] Krishnakant Singh, Simone Schaub-Meyer, and Stefan Roth. Glass: Guided latent slot diffusion for object-centric learning. In *Proceedings of the Computer Vision and Pattern Recognition Conference*, pages 28673–28683, 2025. 1, 3, 5, 8, 2
- [2] Gamaleldin Elsayed, Aravindh Mahendran, Sjoerd Van Steenkiste, Klaus Greff, Michael C Mozer, and Thomas Kipf. Savi++: Towards end-to-end object-centric learning from real-world videos. *Advances in Neural Information Processing Systems*, 35:28940–28954, 2022. 1
- [3] Francesco Locatello, Dirk Weissenborn, Thomas Unterthiner, Aravindh Mahendran, Georg Heigold, Jakob Uszkoreit, Alexey Dosovitskiy, and Thomas Kipf. Object-centric learning with slot attention. *Advances in neural information processing systems*, 33:11525–11538, 2020. 1, 3, 4, 6, 2
- [4] Grkay Aydemir, Weidi Xie, and Fatma Guney. Self-supervised object-centric learning for videos. *Advances in Neural Information Processing Systems*, 36:32879–32899, 2023. 1
- [5] Oriane Simoni, Chloe Sekkat, Gilles Puy, Antonn Vobeck, loi Zablocki, and Patrick Prez. Unsupervised object localization: Observing the background to discover objects. In *Proceedings of the IEEE/CVF conference on computer vision and pattern recognition*, pages 3176–3186, 2023. 1, 7, 8
- [6] Pinzhuo Tian, Shengjie Yang, Hang Yu, and Alex Kot. Pay attention to the foreground in object-centric learning. In *Proceedings of the Computer Vision and Pattern Recognition Conference*, pages 30281–30290, 2025. 1, 3, 4, 6, 7, 8, 2
- [7] Ioannis Kakogeorgiou, Spyros Gidaris, Konstantinos Karantzas, and Nikos Komodakis. Spot: Self-training with patch-order permutation for object-centric learning with autoregressive transformers. In *Proceedings of the IEEE/CVF Conference on Computer Vision and Pattern Recognition*, pages 22776–22786, 2024. 3, 4, 6, 7, 8, 2
- [8] Maximilian Seitzer, Max Horn, Andrii Zadaianchuk, Dominik Zietlow, Tianjun Xiao, Carl-Johann Simon-Gabriel, Tong He, Zheng Zhang, Bernhard Schlkopf, Thomas Brox, et al. Bridging the gap to real-world object-centric learning. *arXiv preprint arXiv:2209.14860*, 2022. 1, 3, 5, 6, 7, 8, 2
- [9] Robin Rombach, Andreas Blattmann, Dominik Lorenz, Patrick Esser, and Bjrn Ommer. High-resolution image synthesis with latent diffusion models. In *Proceedings of the IEEE/CVF conference on computer vision and pattern recognition*, pages 10684–10695, 2022. 2
- [10] Junnan Li, Dongxu Li, Silvio Savarese, and Steven Hoi. Blip-2: Bootstrapping language-image pre-training with frozen image encoders and large language models. In *International conference on machine learning*, pages 19730–19742. PMLR, 2023. 2
- [11] Alexey Dosovitskiy. An image is worth 16x16 words: Transformers for image recognition at scale. *arXiv preprint arXiv:2010.11929*, 2020. 2
- [12] Xudong Wang, Rohit Girdhar, Stella X Yu, and Ishan Misra. Cut and learn for unsupervised object detection and instance segmentation. In *Proceedings of the IEEE/CVF conference on computer vision and pattern recognition*, pages 3124–3134, 2023. 2, 3, 5, 7, 1
- [13] Yangtao Wang, Xi Shen, Yuan Yuan, Yuming Du, Maomao Li, Shell Xu Hu, James L Crowley, and Dominique Vaufreydaz. Tokencut: Segmenting objects in images and videos with self-supervised transformer and normalized cut. *IEEE transactions on pattern analysis and machine intelligence*, 45(12):15790–15801, 2023. 2, 4, 5, 7, 1
- [14] Mathilde Caron, Hugo Touvron, Ishan Misra, Herv Jgou, Julien Mairal, Piotr Bojanowski, and Armand Joulin. Emerging properties in self-supervised vision transformers. In *Proceedings of the IEEE/CVF international conference on computer vision*, pages 9650–9660, 2021. 2
- [15] Oriane Simoni, Gilles Puy, Huy V Vo, Simon Roburin, Spyros Gidaris, Andrei Bursuc, Patrick Prez, Renaud Marlet, and Jean Ponce. Localizing objects with self-supervised transformers and no labels. *arXiv preprint arXiv:2109.14279*, 2021. 2
- [16] Xinlong Wang, Zhiding Yu, Shalini De Mello, Jan Kautz, Anima Anandkumar, Chunhua Shen, and Jose M Alvarez. Freesolo: Learning to segment objects without annotations. In *Proceedings of the IEEE/CVF conference on computer vision and pattern recognition*, pages 14176–14186, 2022. 2
- [17] Xinlong Wang, Rufeng Zhang, Chunhua Shen, Tao Kong, and Lei Li. Solo: A simple framework for instance segmentation. *IEEE transactions on pattern analysis and machine intelligence*, 44(11):8587–8601, 2021. 2
- [18] Wouter Van Gansbeke, Simon Vandenhende, and Luc Van Gool. Discovering object masks with transformers for unsupervised semantic segmentation. *arXiv preprint arXiv:2206.06363*, 2022. 2

- [19] Dantong Niu, Xudong Wang, Xinyang Han, Long Lian, Roei Herzig, and Trevor Darrell. Unsupervised universal image segmentation. In *Proceedings of the IEEE/CVF conference on computer vision and pattern recognition*, pages 22744–22754, 2024. 2
- [20] Huankang Guan, Jiaying Lin, and Rynson WH Lau. A contrastive-learning framework for unsupervised salient object detection. *IEEE Transactions on Image Processing*, 2025. 2
- [21] Christopher P Burgess, Loic Matthey, Nicholas Watters, Rishabh Kabra, Irina Higgins, Matt Botvinick, and Alexander Lerchner. Monet: Unsupervised scene decomposition and representation. *arXiv preprint arXiv:1901.11390*, 2019. 3
- [22] Klaus Greff, Raphaël Lopez Kaufman, Rishabh Kabra, Nick Watters, Christopher Burgess, Daniel Zoran, Loic Matthey, Matthew Botvinick, and Alexander Lerchner. Multi-object representation learning with iterative variational inference. In *International conference on machine learning*, pages 2424–2433. PMLR, 2019. 3
- [23] Martin Engelcke, Adam R Kosiorek, Oiwi Parker Jones, and Ingmar Posner. Genesis: Generative scene inference and sampling with object-centric latent representations. *arXiv preprint arXiv:1907.13052*, 2019. 3, 2
- [24] Yanbo Wang, Letao Liu, and Justin Dauwels. Slot-vae: Object-centric scene generation with slot attention. In *International Conference on Machine Learning*, pages 36020–36035. PMLR, 2023. 3
- [25] Yu Zhang, Songlin Yang, Rui-Jie Zhu, Yue Zhang, Leyang Cui, Yiqiao Wang, Bolun Wang, Freda Shi, Bailin Wang, Wei Bi, et al. Gated slot attention for efficient linear-time sequence modeling. *Advances in Neural Information Processing Systems*, 37:116870–116898, 2024.
- [26] Minhyeok Lee, Suhwan Cho, Dogyoon Lee, Chaewon Park, Jungho Lee, and Sangyoun Lee. Guided slot attention for unsupervised video object segmentation. In *Proceedings of the IEEE/CVF conference on computer vision and pattern recognition*, pages 3807–3816, 2024.
- [27] Jindong Jiang, Fei Deng, Gautam Singh, and Sungjin Ahn. Object-centric slot diffusion. In *Proceedings of the 37th International Conference on Neural Information Processing Systems*, pages 8563–8601, 2023. 6, 8, 2
- [28] Ziyi Wu, Jingyu Hu, Wuyue Lu, Igor Gilitschenski, and Animesh Garg. Slotdiffusion: Object-centric generative modeling with diffusion models. *Advances in Neural Information Processing Systems*, 36:50932–50958, 2023. 3, 4
- [29] Gautam Singh, Fei Deng, and Sungjin Ahn. Illiterate dall-e learns to compose. *arXiv preprint arXiv:2110.11405*, 2021. 3, 6, 2
- [30] Ke Fan, Zechen Bai, Tianjun Xiao, Tong He, Max Horn, Yanwei Fu, Francesco Locatello, and Zheng Zhang. Adaptive slot attention: Object discovery with dynamic slot number. In *Proceedings of the IEEE/CVF Conference on Computer Vision and Pattern Recognition*, pages 23062–23071, 2024. 3
- [31] Rongzhen Zhao, Yi Zhao, Juho Kannala, and Joni Pajarinen. Slot attention with re-initialization and self-distillation. In *Proceedings of the 33rd ACM International Conference on Multimedia*, pages 4185–4192, 2025. 3, 6
- [32] Kyunghyun Cho, Bart Van Merriënboer, Caglar Gulcehre, Dzmitry Bahdanau, Fethi Bougares, Holger Schwenk, and Yoshua Bengio. Learning phrase representations using rnn encoder-decoder for statistical machine translation. *arXiv preprint arXiv:1406.1078*, 2014. 4, 1
- [33] Nick Watters, Loic Matthey, Chris P Burgess, and Alexander Lerchner. Spatial broadcast decoder: A simple architecture for disentangled representations in vaes. *ICLR Workshop on Learning from Limited Labeled Data*, 2019. 4, 1
- [34] Gautam Singh, Yi-Fu Wu, and Sungjin Ahn. Simple unsupervised object-centric learning for complex and naturalistic videos. *Advances in Neural Information Processing Systems*, 35:18181–18196, 2022. 4
- [35] David Arthur and Sergei Vassilvitskii. k-means++: The advantages of careful seeding. Technical report, Stanford, 2006. 4, 7, 1
- [36] Subhransu Maji, Nisheeth K Vishnoi, and Jitendra Malik. Biased normalized cuts. In *CVPR 2011*, pages 2057–2064. IEEE, 2011. 4, 5
- [37] Harold W Kuhn. The hungarian method for the assignment problem. *Naval research logistics quarterly*, 2(1-2):83–97, 1955. 5
- [38] Klaus Greff, Francois Belletti, Lucas Beyer, Carl Doersch, Yilun Du, Daniel Duckworth, David J Fleet, Dan Gnanaprasam, Florian Golemo, Charles Herrmann, et al. Kubric: A scalable dataset generator. In *Proceedings of the IEEE/CVF conference on computer vision and pattern recognition*, pages 3749–3761, 2022. 5, 2
- [39] Tsung-Yi Lin, Michael Maire, Serge Belongie, James Hays, Pietro Perona, Deva Ramanan, Piotr Dollár, and C Lawrence Zitnick. Microsoft coco: Common objects in context. In *European conference on computer vision*, pages 740–755. Springer, 2014. 5, 2
- [40] Mark Everingham, Luc Van Gool, Christopher KI Williams, John Winn, and Andrew Zisserman. The pascal visual object classes (voc) challenge. *International journal of computer vision*, 88(2):303–338, 2010. 5, 2
- [41] Laurynas Karazija, Iro Laina, and Christian Rupprecht. Clevrtex: A texture-rich benchmark for unsupervised multi-object segmentation. *arXiv preprint arXiv:2111.10265*, 2021. 5, 8, 2, 3
- [42] Shuai Shao, Zeming Li, Tianyuan Zhang, Chao Peng, Gang Yu, Xiangyu Zhang, Jing Li, and Jian Sun. Objects365: A large-scale, high-quality dataset for object detection. In *Proceedings of the IEEE/CVF international conference on computer vision*, pages 8430–8439, 2019. 5, 8, 3
- [43] Maxime Oquab, Timothée Darcet, Théo Moutakanni, Huy Vo, Marc Szafraniec, Vasil Khalidov, Pierre Fernandez, Daniel Haziza, Francisco Massa, Alaaeldin El-Nouby, et al. Dinov2: Learning robust visual features without supervision. *arXiv preprint arXiv:2304.07193*, 2023. 6, 1, 2
- [44] Yifan Wang, Wenbo Zhang, Lijun Wang, Ting Liu, and Huchuan Lu. Multi-source uncertainty mining for deep unsupervised saliency detection. In *Proceedings of the IEEE/CVF conference on computer vision and pattern recognition*, pages 11727–11736, 2022. 7

- [45] Gyungin Shin, Samuel Albanie, and Weidi Xie. Unsupervised salient object detection with spectral cluster voting. In *Proceedings of the IEEE/CVF Conference on Computer Vision and Pattern Recognition*, pages 3971–3980, 2022. [7](#)
- [46] Rajeev Yasarla, Renliang Weng, Wongun Choi, Vishal M Patel, and Amir Sadeghian. 3sd: Self-supervised saliency detection with no labels. In *Proceedings of the IEEE/CVF Winter Conference on Applications of Computer Vision*, pages 313–322, 2024. [7](#)
- [47] Yin Li, Xiaodi Hou, Christof Koch, James M Rehg, and Alan L Yuille. The secrets of salient object segmentation. In *Proceedings of the IEEE conference on computer vision and pattern recognition*, pages 280–287, 2014. [7](#)
- [48] Xinlei Chen, Saining Xie, and Kaiming He. An empirical study of training self-supervised vision transformers. In *Proceedings of the IEEE/CVF international conference on computer vision*, pages 9640–9649, 2021. [2](#)
- [49] Kaiming He, Xinlei Chen, Saining Xie, Yanghao Li, Piotr Dollár, and Ross Girshick. Masked autoencoders are scalable vision learners. In *Proceedings of the IEEE/CVF conference on computer vision and pattern recognition*, pages 16000–16009, 2022. [2](#)
- [50] William M Rand. Objective criteria for the evaluation of clustering methods. *Journal of the American Statistical association*, 66(336):846–850, 1971. [2](#)
- [51] Ilya Loshchilov, Frank Hutter, et al. Fixing weight decay regularization in adam. *arXiv preprint arXiv:1711.05101*, 5(5):5, 2017. [2](#)
- [52] Nikhila Ravi, Valentin Gabeur, Yuan-Ting Hu, Ronghang Hu, Chaitanya Ryali, Tengyu Ma, Haitham Khedr, Roman Rädle, Chloe Rolland, Laura Gustafson, et al. Sam 2: Segment anything in images and videos. *arXiv preprint arXiv:2408.00714*, 2024. [3](#)